Metabolite Profiling of *Allium hookeri* Leaves using UPLC-qTOF-MS/MS and Senomorphic Activity of Phenolamides

Thi-Phuong Doan , Mi Zhang , Jin-Pyo An , Jorge-Eduardo Ponce-Zea , Van-Hieu Mai , Byeol Ryu , Eun Jin Park , And Won-Keun Oh *

Posted Date: 17 October 2023

doi: 10.20944/preprints202310.1019.v1

Keywords: Allium hookeri; N-trans-feruloyltyramine; senomorphic effect; SASP inhibitor

Article

Metabolite Profiling of *Allium hookeri* Leaves using UPLC-qTOF-MS/MS and Senomorphic Activity of Phenolamides

Thi-Phuong Doan [1], Mi Zhang [1], Jin-Pyo An [1], Jorge-Eduardo Ponce-Zea [1], Van-Hieu Mai [1], Byeol Ryu [1], Eun Jin Park [1] and Won-Keun Oh [1,*]

[1] Research Institute of Pharmaceutical Sciences, College of Pharmacy, Seoul National University, Seoul 08826, Republic of Korea; phuongdoan@snu.ac.kr (T.P.D); mintazhang@snu.ac.kr (M.Z); ntopjp77@gmail.com (J.P.A); jepz210689@snu.ac.kr (J.E.P); maihieu@snu.ac.kr (V.H.M); estrella56@snu.ac.kr (B.R); eunjin_p@snu.ac.kr (E.J.P); wkoh1@snu.ac.kr (W.K.O)

* Correspondence: wkoh1@snu.ac.kr; Tel.: +82-2-880-7872

Abstract: The plant *Allium hookeri*, belonging to the *Allium* genus, has a history of being used both as a common food ingredient and in herbal medicine. It has recently been reported to have anti-oxidant and anti-inflammatory effects. *A. hookeri* has been also shown to exhibit neuroprotective and anti-neuroinflammatory activities, but the active compounds responsible for these effects have not been identified in previous studies. This study aimed to perform a metabolite profiling using an HRESI-qTOF MS/MS-based molecular networking approach and identify the active compounds from *A. hookeri* that target senescent cell-associated secretory phenotype (SASP) inhibitory effects, which contribute to neuroprotective activities. As a result, ten compounds, including one new flavonoid (**2**) and nine known compounds (**1** and **3**–**10**), were identified, and their biological activity was tested. The most potent compound was *N-trans*-feruloyltyramine (**7**), which inhibited SASP markers and contributed to the senomorphic activities of *A. hookeri*. These findings suggest that the phenolamides from *A. hookeri* could be a promising source of bioactive compounds for preventing senescence-associated diseases.

Keywords: *Allium hookeri*; *N-trans*-feruloyltyramine; senomorphic effect; SASP inhibitor

1. Introduction

The *Allium* genus, the largest within the Amaryllidaceae family, comprises more than 500 species [1], including well-known vegetables like onion (*A. cepa*), garlic (*A. sativum*), chive (*A. schoenoprasum*), leek (*A. ampeloprasum* var. *porrum*), and rakkyo (*A. chinense*) [2]. *Allium hookeri* Thwaites, also referred to as wide-leaf chives or extra-wide-leaf chives, is a herbaceous plant native to regions such as India, Sri Lanka, Myanmar, Bhutan, and southwestern China. It has a long history of culinary and medicinal cultivation in South and southwestern Asia and has recently expanded into southern areas of Korea [3]. The roots of *A. hookeri* have undergone extensive studies, revealing regulatory effects against asthmatic changes [4], antioxidant potentials [5], antimicrobial properties [6], anti-diabetic effects [7,8], immunomodulatory [9], anti-inflammatory [10,11], and bone-forming activities [12]. In addition, the leaves of *A. hoookeri* have been found to exhibit anti-obesity [13], anti-inflammatory, and immunomodulating effects [9]. The phytochemical profile of *A. hookeri* includes sulfur-containing compounds [14], flavonoids [15], fatty acids, phenolic, and polyphenols [5,6,15,16], and essential oils [17]. While numerous activities of *A. hookeri* have been reported, only a limited number of studies have identified a direct link between compounds and their biological activities, such as fatty acid, phenolic, and polyphenols with antimicrobial activity [6], and its phenolic compounds with antioxidant properties [5].

The aging of the global population is becoming an increasingly significant medical concern. While life expectancy has increased in the past century, the additional years gained have not necessarily translated into a state of good health, especially for individuals aged 60 years and older

 doi:10.20944/preprints202310.1019.v1

[18]. In response to the challenges posed by population aging, the World Health Organization (WHO) has formulated a definition of healthy aging, describing it as a process of developing and maintaining functional abilities that contribute to well-being in older age [19]. Furthermore, the United Nations has designated the period from 2021 to 2030 as the UN Decade of Healthy Ageing [18]. The "hallmarks" of aging refer to the accumulation of damages, including genomic instability, telomere attrition, epigenetic alterations, loss of proteostasis, mitochondrial dysfunction, deregulated nutrient sensing, cellular senescence, stem cell exhaustion, and altered intercellular communication [20]. Among these hallmarks, cellular senescence, characterized by irreversible cell cycle arrest, the expression of senescence-associated beta-galactosidase (SA-β-gal) and senescence-associated secretory phenotype (SASP) [21], plays a significant role in complex biological processes related to aging and age-related disorders [22]. As individuals age, senescent cells tend to accumulate in tissues and organs, thereby contributing to the development of age-related diseases [22]. The removal of senescent cells from tissues and organs may represent a crucial strategy for preventing and treating age-related diseases, thereby increasing the health span [20]. Senotherapeutics achieve their effect by targeting two approaches: eliminating senescent cells (senolytics) or inhibiting senescent phenotypes such as SA-β-gal or SASP secretion (senomorphics) [20]. To date, several natural products have been identified as senolytic agents, including quercetin, fisetin, piperlongumine, and the curcumin analog [23]. Additionally, natural senomorphics such as rapamycin, resveratrol, kaempferol, apigenin, and EGCG have been also discovered [24].

In this study, we aimed to identify the phytochemicals present in *A. hookeri*, assess its senomorphic activities, and explore the key compound responsible for the senomorphic effects of *A. hookeri* in LPS-induced NO production and bleomycin-induced senescent model.

2. Materials and Methods

2.1. Materials

Optical rotations were determined using a JASCO P-2000 polarimeter (JASCO International Co. Ltd., Tokyo, Japan). IR spectra were measured with a Nicolet 6700 FT-IR spectrometer (Thermo Electron Corp., Waltham, MA, USA). NMR data analysis was performed with a JNM-ECA 600 MHz spectrometer (Jeol, Japan) coupled with a 5 mm CPTCI cryoprobe (Bruker, Germany). For column chromatography, silica gel (Merck, particle size 63–200 μm) and RP-18 (Merck, particle size 75 μm) were used. Sephadex LH-20 from Sigma-Aldrich (St. Louis, MO, USA) was also used. Thin-layer chromatography (TLC) was conducted using silica gel 60 F_{254} and RP-18 F_{254} plates from Merck. High-performance liquid chromatography (HPLC) was carried out using a Gilson system with a UV detector (at 201 and 254nm) and an Optima Pak C_{18} column (10 × 250 mm, particle size 5 μm, RS Tech, Korea).

2.2. Plant Material

A. hookeri was purchased from the commercial stores in March 2019 and was authenticated by Professor W. K. Oh. The samples were dried at room temperature, and a voucher specimen (2019-SNU-12) was deposited in the herbarium at the College of Pharmacy, Seoul National University, Seoul, Korea.

2.3. UHPLC-qTOF-MS/MS Experiments

The chemical profiling of *A. hookeri* was performed using an Agilent 6530 Q-TOF mass spectrometer equipped with an Agilent 1260 Infinity UPLC (Agilent Technologies, Santa Clara, CA, USA). A Waters Acquity UHPLC® BEH C18 (100 mm × 2.1 mm, 1.7 μm) column was used for chromatographic analysis, and the column temperature was maintained at 40 °C. LC-MS/MS analyses were performed using fast data-dependent acquisition (DDA) mode. The chromatographic separation was performed using a linear gradient of H_2O (with 0.1% aqueous formic acid, A) and acetonitrile (with 0.1% aqueous formic acid, B) as follows: 0–20 min, 10–90% B; 20.1–22 min, 100% B; and 22.1–24.0 min, 10% A. The ESI conditions were set to the following parameters: an untargeted

Preprints (www.preprints.org) | NOT PEER-REVIEWED | Posted: 17 October 2023 doi:10.20944/preprints202310.1019.v1

MS scan from 100 to 1500 *m/z* in positive and negative ion modes. The instrumental parameters were set as follows: sheath gas temperature, 350 °C; gas flow, 10L/min; nebulizer pressure, 30 psig. The scan source parameters include VCap (4000 V), nozzle voltage (1000 V), fragmentor (180 V), skimmer (65 V), and octopole RF peak voltages (750 V). A collision energy of 50 eV was also used.

2.4. Sample Preparation of A. hookeri for MS/MS Analysis

Fresh whole *A. hooker* (5 g) was extracted by sonication for 1.5 h with 20 mL of 70% EtOH (x 3 times) at room temperature. The total extracts were combined, dried under a vacuum pump, and then sequentially chromatographed using Sep-pak column eluting with H_2O, 25%, 50%, 75%, 90%, and 100% MeOH/H_2O. All samples were dried and diluted to a final concentration of 2.0 mg/mL with HPLC-grade MeOH for further analysis. All samples were filtered through a 0.20 μm membrane filter (Advantec, Tokyo Roshi Kaisha, Japan), and 2 μL of each sample was injected into the mass spectrometer.

2.5. Extraction and Isolation

The air-dried leaves of *A. hookeri* were cut into small pieces and extracted with 70% EtOH using sonication for 90 min (three times) under room temperature. The resulting combined extract was then suspended in water and applied to a Daion HP-20 column chromatography (CC). Elution was achieved using a MeOH/H_2O gradient, resulting in the separation of the extract into three different fractions: H1 (50% MeOH), H2 (75% MeOH), H3 (100% MeOH). Fraction H3 was further subjected to normal phase silica gel CC, eluting with an elution gradient of EtOAc/MeOH (2:1, 1:1, to 0:1) to obtain four fractions (N1-N4). Fraction N2, exhibiting the target peaks corresponding to flavones and amides, was further chromatographed on a reverse-phase C_{18} column with a mobile phase of 50–100% MeOH in water to give 18 sub-fractions (R1-R18). Sub-fraction R2 was then processed through a Sephadex LH-20 column, with elution achieved using 100% MeOH, yielding ten fractions (L1-L10). Fraction L2 was subjected to purification via an HPLC system equipped with an RP C_{18} column, ultimately resulting in the isolation of compound **4**, while fraction L5 provided compound **2**. Fraction L4 was further processed through an MPLC column, separating it into ten sub-fractions (M1-M10). After the purification of sub-fraction M3 through the HPLC system, compounds **1**, **3**, and **7** were obtained. Similarly, compounds **9** and **10** were yielded from sub-fraction M5 through the HPLC system, while sub-fraction M7 contained compounds **5**, **6**, and **8**.

2.5.1. Physicochemical Properties of Isolated Compounds

Apigenin-7-*O*-glucuronide (**1**): Pale yellow amorphous powder; $[\alpha]_D^{25}$= – 32.1 (*c* 0.1, MeOH); IR (KBr) ν_{max} 3298, 2908, 2818, 1736, 1662, 1607, 1498, 1443, 1349, 1299, 1250, 1175, 1105, 1086, 1061, 1026, 833, 763, 679, 629 cm^{-1}; ^1H NMR (pyridine-d_5, 600 MHz) and ^{13}C NMR (pyridine-d_5, 150 MHz): Figures S14 and S15; HRESIMS: found *m/z* 477.0899 $[M + H]^+$ (calcd for $C_{21}H_{19}O_{11}$ at 477.0927, *m/z* error – 5.87 ppm).

Apigenin-7-*O*-[α-L-rhamnopyranosyl(1 → 2)]β-D-glucuronic acid methyl ester (**2**): Pale yellow amorphous powder; $[\alpha]_D^{25}$= – 13.4 (*c* 0.1, MeOH); UV (MeOH) λ_{max} (log ε); IR (KBr) ν_{max} 3370, 2926, 2382, 2357, 2307, 1748, 1658, 1608, 1513, 1443, 1344, 1298, 1248, 1179, 1099, 949, 835, 679, 604 cm^{-1}; ^1H NMR (pyridine-d_5, 600 MHz) and ^{13}C NMR (pyridine-d_5, 150 MHz): Table 1; HRESIMS: found *m/z* 607.1637 $[M + H]^+$ (calcd. for $C_{28}H_{29}O_{15}$ at 605.1663, *m/z* error – 4.28 ppm).

Table 1. ^1H and ^{13}C NMR data of compound **2.**

Pos.	2	
	δ_C [a]	δ_H (*J* in Hz)[b]
2	165.5	
3	104.5	6.93, s
4	183.3	
5	158.3	
6	95.6	7.20, overlap.

Preprints (www.preprints.org) | NOT PEER-REVIEWED | Posted: 17 October 2023 doi:10.20944/preprints202310.1019.v1

7	163.7	
8	100.8	7.04, s
9	163.4	
10	107.4	
1'	122.4	
2'	129.5	7.85, d (5.1)
3'	117.4	7.19, overlap.
4'	163.3	
5'	117.4	
6'	129.5	
1''	100.0	6.03, d (7.3)
2''	77.8	4.65, t (7.8)
3''	78.7	4.47, t (8.8)
4''	73.3	4.52, t (8.8)
5''	77.5	4.88, d (8.5)
-C=O	170.4	
-COO**C**H$_3$	52.6	3.62, s
4'-OCH$_3$		
1'''	103.1	6.45, s
2'''	72.9	4.84, br s
3'''	73.2	4.58, d (7.7)
4'''	74.5	4.38, t (9.1)
5'''	70.6	4.80, m
6'''	19.4	1.85, d (6.0)

[a] Recorded in Pyridine-d_5 at 600 MHz, [b] Recorded in Pyridine-d_5 at 150 MHz.

Apigenin 7-*O*-glucuronide methyl ester (**3**): Pale yellow amorphous powder; $[\alpha]_D^{25} = -19.8$ (*c* 0.1, MeOH); IR (KBr) ν_{max} 3725, 3630, 3600, 3316, 2926, 2387, 2352, 2312, 1752, 1618, 1588, 1523, 1468, 1363, 1339, 1248, 1174, 1044, 835, 684, 670, 645 cm^{-1}; ^{1}H NMR (DMSO-d_6, 600 MHz) and ^{13}C NMR (DMSO-d_6, 150 MHz): Figures S17 and S18; HRESIMS: found *m*/*z* 461.1055 [M + H]$^+$ (calcd. for $C_{22}H_{21}O_{11}$ at 461.1084, *m*/*z* error – 6.29 ppm).

Chrysoeriol-7-*O*-*β*-D-glucuronide (**4**): Pale yellow amorphous powder; $[\alpha]_D^{25} = +30.7$ (*c* 0.1, MeOH); UV (MeOH) λ_{max} (log ε) 252 (– 1.95), 350 (– 1.85); IR (KBr) ν_{max} 3730, 3620, 3595, 3300, 2946, 2387, 2307, 1748, 1613, 1503, 1418, 1333, 1174, 1039, 689, 670, 645 cm^{-1}; ^{1}H NMR (DMSO-d_6, 500 MHz) and ^{13}C NMR (DMSO-d_6, 125 MHz): Figures S22 and S23; HRESIMS: found *m*/*z* 477.1032 [M + H]$^+$ (calcd. for $C_{22}H_{21}O_{12}$ at 477.1033, *m*/*z* error – 0.2 ppm).

Chrysoeriol-7-*O*-*β*-D-glucuronic acid methyl ester (**5**): Pale yellow amorphous powder; $[\alpha]_D^{25} = -64.7$ (*c* 0.1, MeOH); UV (MeOH) λ_{max} (log ε) 203 (– 0.90), 252 (– 0.67), 348 (– 0.52); IR (KBr) ν_{max} 3725, 3700, 3625, 3595, 3306, 2966, 2387, 2362, 2342, 2307, 1748, 1513, 1418, 1363, 1333, 1049, 1034, 1014, 689, 674, 649, 615 cm^{-1}; ^{1}H NMR (DMSO-d_6, 600 MHz) and ^{13}C NMR (DMSO-d_6, 150 MHz): Figures S27 and S28; HRESIMS: found *m*/*z* 491.1193 [M + H]$^+$ (calcd. for $C_{23}H_{23}O_{12}$ at 491.1190, *m*/*z* error 0.61 ppm).

Paprazine (**6**): Pale yellow amorphous powder; $[\alpha]_D^{25} = -18.1$ (*c* 0.1, MeOH); IR (KBr) ν_{max} 3717, 3696, 3627, 2972, 2386, 2351, 2302, 146, 1508, 1220, 1051, 818, 673 cm^{-1}; ^{1}H NMR (DMSO-d_6, 500 MHz) and ^{13}C NMR (DMSO-d_6, 125 MHz): Figures S31, S32; HRESIMS: found *m*/*z* 284.1281 [M + H]$^+$ (calcd. for $C_{17}H_{18}NO_3$ at 284.1287, *m*/*z* error – 2.11 ppm).

N-*trans*-feruloyltyramine (**7**): Pale yellow amorphous powder; $[\alpha]_D^{25} = -24.7$ (*c* 0.1, MeOH); IR (KBr) ν_{max} 3731, 3702, 3627, 3597, 3344, 2942, 2381, 2357, 2307, 1592, 1508, 1265, 1225, 1031, 823, 679 cm^{-1}; ^{1}H NMR (DMSO-d_6, 400 MHz) and ^{13}C NMR (DMSO-d_6, 100 MHz): Figures S35, S36; HRESIMS: found *m*/*z* 314.1381 [M + H]$^+$ (calcd. for $C_{18}H_{20}NO_4$ at 314.1392, *m*/*z* error – 3.50 ppm).

N-*trans*-feruloyl-3-*O*-methyldopamine (**8**): Pale yellow amorphous powder; $[\alpha]_D^{25} = -13.0$ (*c* 0.1, MeOH); UV (MeOH) λ_{max} (log ε) 240 (– 1.60), 290 (– 1.54), 318 (– 1.49); IR (KBr) ν_{max} 3737, 3726, 3702, 3627, 3592, 3305, 2972, 2938, 2381, 2357, 2312, 1752, 1602, 1508, 1269, 1220, 1126, 1036, 689, 669 cm^{-1}; ^{1}H NMR (DMSO-d_6, 600 MHz) and ^{13}C NMR (DMSO-d_6, 150 MHz): Figures S40, S41; HRESIMS: found *m*/*z* 344.1427 [M + H]$^+$ (calcd. for $C_{19}H_{21}NO_5$ at 344.1420, *m*/*z* error 2.03 ppm).

Preprints (www.preprints.org) | NOT PEER-REVIEWED | Posted: 17 October 2023 doi:10.20944/preprints202310.1019.v1

5,7,4′-Trimethoxyflavone (**9**): Pale yellow amorphous powder; $[\alpha]_D^{25}$= – 49.1 (*c* 0.1, MeOH); UV (MeOH) λ_{max} (log ε) 230 (– 0.85), 265 (– 0.62), 328 (– 0.56); IR (KBr) ν_{max} 3349, 2942, 2351, 1642, 1607, 1518, 1458, 1424, 1349, 1255, 1220, 1181, 1160, 1126, 1091, 1051, 1026, 837, 673 cm^{-1}; ^1H NMR (DMSO-d_6, 600 MHz) and ^{13}C NMR (DMSO-d_6, 150 MHz): Figures S45, S46; HRESIMS: found *m*/*z* 313.1084 $[M + H]^+$ (calcd. for $C_{18}H_{17}O_5$ at 313.1076, *m*/*z* error 2.6 ppm).

Diosgenin-3-*O*-[[β-D-glucopyranosyl(1 → 4)]-α-L-rhamnopyranosyl(1 → 4)]-[α-L-rhamnopyranosyl(1→2)]]β-D-glucopyranoside (**10**): Pale yellow amorphous powder; $[\alpha]_D^{25}$= – 39.4 (*c* 0.1, MeOH); IR (KBr) ν_{max} 3414, 2933, 2898, 2362, 2312, 1542, 1458, 1378, 1309, 1135, 1036, 907, 828, 673, 645 cm^{-1}; ^1H NMR (pyridine-d_5, 500 MHz) and ^{13}C NMR (pyridine-d_5, 125 MHz): Figures S49, S50; HRESIMS: found *m*/*z* 1031.5406 $[M + H]^+$ (calcd. for $C_{28}H_{29}O_{15}$ at 1031.5427, *m*/*z* error – 2.04 ppm).

2.6. Cell Culture

RAW264.7 cells were kindly provided by Prof. SH Sung at Seoul National University, Seoul, Korea. These cells were cultured in Dulbecco's modified Eagle medium (DMEM) (HyClone, Logan, UT, USA) at 37 °C in 5% CO_2, supplemented with 10% fetal bovine serum (FBS), 100 units/mL of penicillin, and 100 μg/mL of streptomycin. Subculturing of the cells was performed every 48 hours.

2.7. LPS-Induced NO Production and Cell Viability

Cells were plated and incubated overnight in 96-well plates at a density of 5×10^4 cells/well. After cells were attached to the wells, lipopolysaccharide (LPS, 1 μg/ mL) was added with and without the isolated compounds. After treatment of the isolated compounds, nitrite levels were assessed using the Griess reagent method, which consists of a 1:1 ratio of solution A (1% sulfanilamide) and solution B (5% phosphoric acid with 0.1% naphthyl ethylenediamine-HCl). The absorbance was measured at 540 nm using a microplate reader (VersaMaxTM, Randor, PA, USA). Nitrite levels in the samples were evaluated using a standard nitrite (Kim et al., 2003) and cell viability was assessed using an MTT assay.

2.8. Bleomycin-Induced Senescent Model

The human lung carcinoma epithelial cell line (A549), a type II epithelial-like cell line, was purchased from the Korean Cell Line Bank (Seoul, Korea) and maintained in RPMI 1640 medium (Welgene, Deajeon, Korea) supplemented with 10% FBS (Gibco), 100 U of penicillin, and 100 *m*g/mL of streptomycin (Hyclone). For experiments involving bleomycin-induced senescence, A549 cells were exposed to 5 *m*g/ml of bleomycin (Tokyo Chemical Industry) for 4 days in a growth medium. To evaluate the senomorphic effect, cells were co-treated with 5 *m*g/ml of bleomycin and the indicated compounds for 6 days. Then, RNA was extracted to compare the aging-related markers after bleomycin-induced senescence.

2.8.1. Senescence-Associated β-Galactosidase Staining

Cells were stained using the Senescence β-Glactosidase Staining Kit (#9860, Cell Signaling Technology, Denver, MA) following the manufacturer's instructions. After staining, cell samples were observed under an Olympus ix70 microscope (Olympus Corporation, Tokyo, Japan).

2.9. RNA Extraction and Quantitative Real-Time Polymerase Chain Reaction (qRT-PCR)

Human dermal fibroblast (HDF) cells were seeded in a 6-well plate at a density of 80,000 per well. After a 3-day treatment, 250 μL of TRIzol reagent (Invitrogen, USA) was added to each well to extract the total RNA. For further cDNA synthesis, 1 μg of total RNA and an M-MLV Reverse Transcriptase kit (Bioneer, Korea) were used. A 20 μL reaction was performed and then diluted to 100 μL, which was used as a template in the following real-time qPCR reactions. Real-time qPCR was conducted using AccuPower® 2X GreenStar™ qPCR Master Mix (Bioneer). All reactions were performed in triplicate and the expression levels of all markers were normalized to the expression level of 18s ribosomal RNA.

Preprints (www.preprints.org) | NOT PEER-REVIEWED | Posted: 17 October 2023 doi:10.20944/preprints202310.1019.v1

2.10. Statistical Analyses

The data were analyzed using GraphPad PRISM (GraphPad Software, Inc., La Jolla, CA, USA) and are presented as the mean ± standard deviation (SD) of triplicate experiments. Analysis of variance (ANOVA) was employed to justify comparisons between group means, and Tukey's multiple comparison test was performed for post hoc analysis. A significance level of $p < 0.05$ was considered statistically significant.

3. Results

3.1. Feature-Based Molecular Networking of the A. hookeri Leaves Extract

The leaves of *A. hookeri* were extracted by 70% EtOH (3 times) to obtain the total crude extract. After being dried under a vacuum pump, the extract was suspended in water and loaded into a Daion HP-20 chromatography column. The column was eluted with 50%, 75%, and 100% MeOH/H_2O to obtain three fractions (H1–H3). The 70% EtOH extract and three fractions were dried and prepared at a concentration of 2mg/mL for HRESI-qTOF-MS/MS measurement in both positive and negative modes. The mass data were analyzed using MassHunter software and the results were shown in Figure S1 (Supplementary Information) for positive mode. For molecular networking analysis, all data (in positive mode) were pre-processed using Mzmine 3 to obtain .csv and .mgf files. These files were then uploaded to the GNPS platform to create the feature-based molecular networking (FBMN). The result was visualized using Cytoscape, as shown in Figure S2 (Supplementary Information) for the full network, and Figure 1A for clusters of interest.

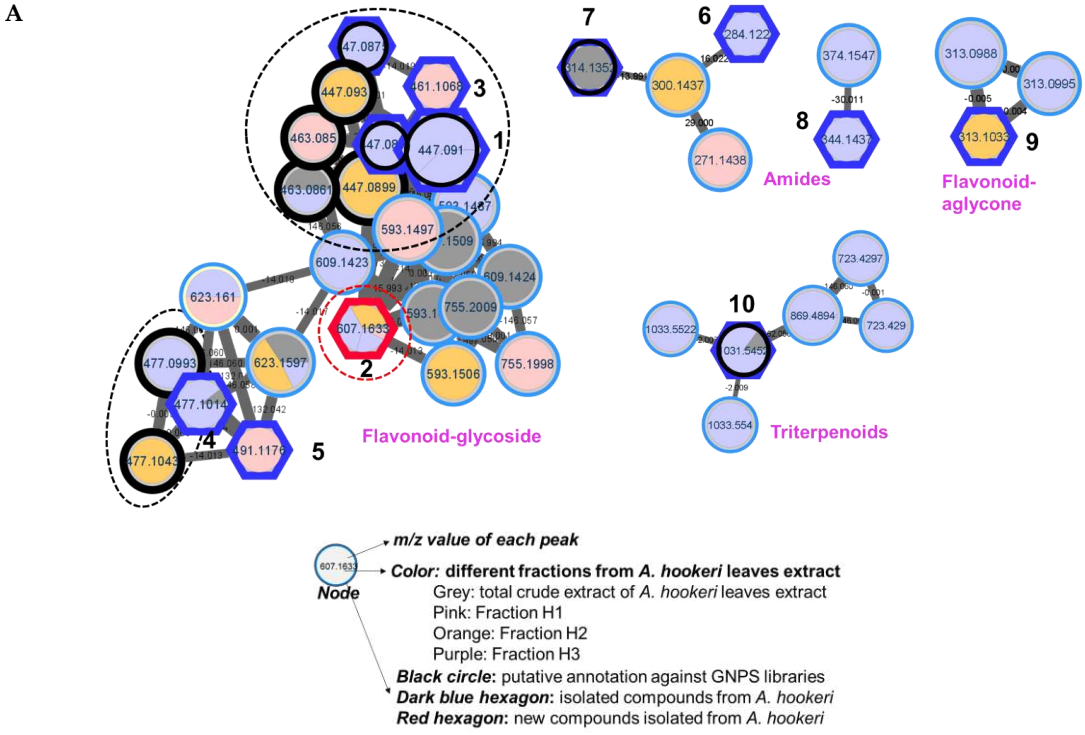

Preprints (www.preprints.org) | NOT PEER-REVIEWED | Posted: 17 October 2023 doi:10.20944/preprints202310.1019.v1

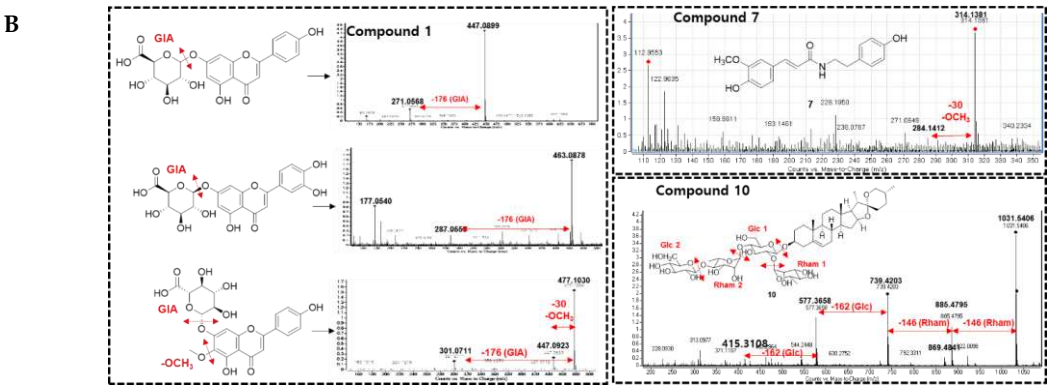

Figure 1. (A) Molecular networking of crude extract, EtOAc, and *n*-BuOH fractions from leaves of *Allium hookeri* using HRESI-qTOF-MS/MS data recorded in positive mode. The black frame was assigned by GNPS and blue frame for the accuracy of the MN was confirmed by isolating compounds (**1**–**10**) from each cluster and confirming their structures to the physicochemical properties of reported compounds using spectroscopic methods. The red frame shows a new compound **2**, which was first identified from this plant. (B) Analysis of cluster of interest related to flavonoid glycoside suggested by molecular networking.

As shown in Figure 1A, four clusters of interest were identified, including flavonoids-glycosides, amides, triterpenoids, and others. In the flavonoid-glycosides cluster, three compounds were annotated by the GNPS platform against the online database of GNPS, including apigenin-7-*O*-glucuronide (*m*/*z* 447 Da), (2S,3S,4S,5R,6S)-6-[2-(3,4-dihydroxyphenyl)-5-hydroxy-4-oxochromen-7-yl]oxy-3,4,5-trihydroxyoxane-2-carboxylic acid (*m*/*z* 463 Da), and (2S,3S,4S,5R,6S)-3,4,5-trihydroxy-6-[5-hydroxy-2-(4-hydroxyphenyl)-6-methoxy-4-oxochromen-7-yl]oxyoxane-2-carboxylic acid (*m*/*z* 477 Da). The amide cluster displayed the presence of moupinamide (N-*trans*-feruloyltyramine) (*m*/*z* 314 Da), while the triterpenoids group was suggested to contain the compound *β*-D-glucopyranoside, (3β,22β,25R)-26-(*β*-D-glucopyranosyloxy)-22-hydroxyfurost-5-en-3-yl *O*-6-deoxy-*α*-L-mannopyranosyl-(1->2)-*O*-[6-deoxy-*α*-L-mannopyranosyl-(1->4)] (*m*/*z* 1031 Da). The mass data for each putative compound was analyzed in detail to understand their fragmentation pattern, which is exhibited in Figure 1B. Among these annotated compounds, compounds **1, 7**, and **10** were isolated to confirm their structures.

Compound **1**, observed within the flavonoid-glycoside cluster at an *m*/*z* value of 447.0899 Da (Figure 1A), was characterized as apigenin-7-*O*-glucuronide through comparison against GNPS libraries matching. Additionally, its identification was corroborated via nuclear magnetic resonance (NMR) spectroscopic, referencing previously documented literature data [25]. Mass fragmentation analysis of compound **1** and the other identified nodes (black circle) within the flavonoid-glycosides cluster revealed the consistent presence of a glucuronic acid moiety, as evidenced by distinct *m*/*z* differences of 176 Da in their primary fragments (Figure 1B). A node of *m*/*z* 461.1068 Da was not assigned against GNPS libraries. However, this node was clustered in the same group as compound **1,** and the mass difference of 14 Da suggests that an additional methoxy (-OCH_3) replaced a hydroxy group. Compound **3** was then isolated, and the structure was confirmed as apigenin 7-*O*-glucuronide methyl ester by NMR spectra, compared to the literature [26], and mass fragmentation analysis (Figure 3A). Similarly, compound **4**, which shared the same *m*/*z* value but different retention time as the annotated compound (2*S*,3*S*,4*S*,5*R*,6*S*)-3,4,5-trihydroxy-6-[5-hydroxy-2-(4-hydroxyphenyl)-6-methoxy-4-oxochromen-7-yl]oxyoxane-2-carboxylic acid was further confirmed by its mass fragments and NMR data to be chrysoeriol-7-*O*-*β*-D-glucuronide [27]. The mass data of compound **5** (*m*/*z* 491 Da) showed a loss of 191 Da, which is characteristic of a methyl-GlA, a methoxy (30 Da), and a hydroxy (17 Da). Additionally, a mass difference of 14 Da compared to compound **4** indicated that **5** had an additional methyl group attached in the GlA unit to form methyl GlA ester. Compound **5** was also purified, and the structure was confirmed by NMR and compared to the reference to be

Preprints (www.preprints.org) | NOT PEER-REVIEWED | Posted: 17 October 2023 doi:10.20944/preprints202310.1019.v1

chrysoeriol-7-*O*-*β*-D-glucuronic acid methyl ester [28]. Compound **9**, situated within a flavonoid-aglycone cluster (Figure 1A) and exhibiting an observed *m*/*z* value of 313.1084 Da, was conclusively identified as 5,7,4′-trimethoxyflavone. This determination was based on its NMR spectroscopic data, well matching with the literature report [29], and further supported by mass fragmentation analysis, which revealed the presence of a fragment with an *m*/*z* of 287 Da $[M - OCH_3]^+$ as shown in Figure 3A.

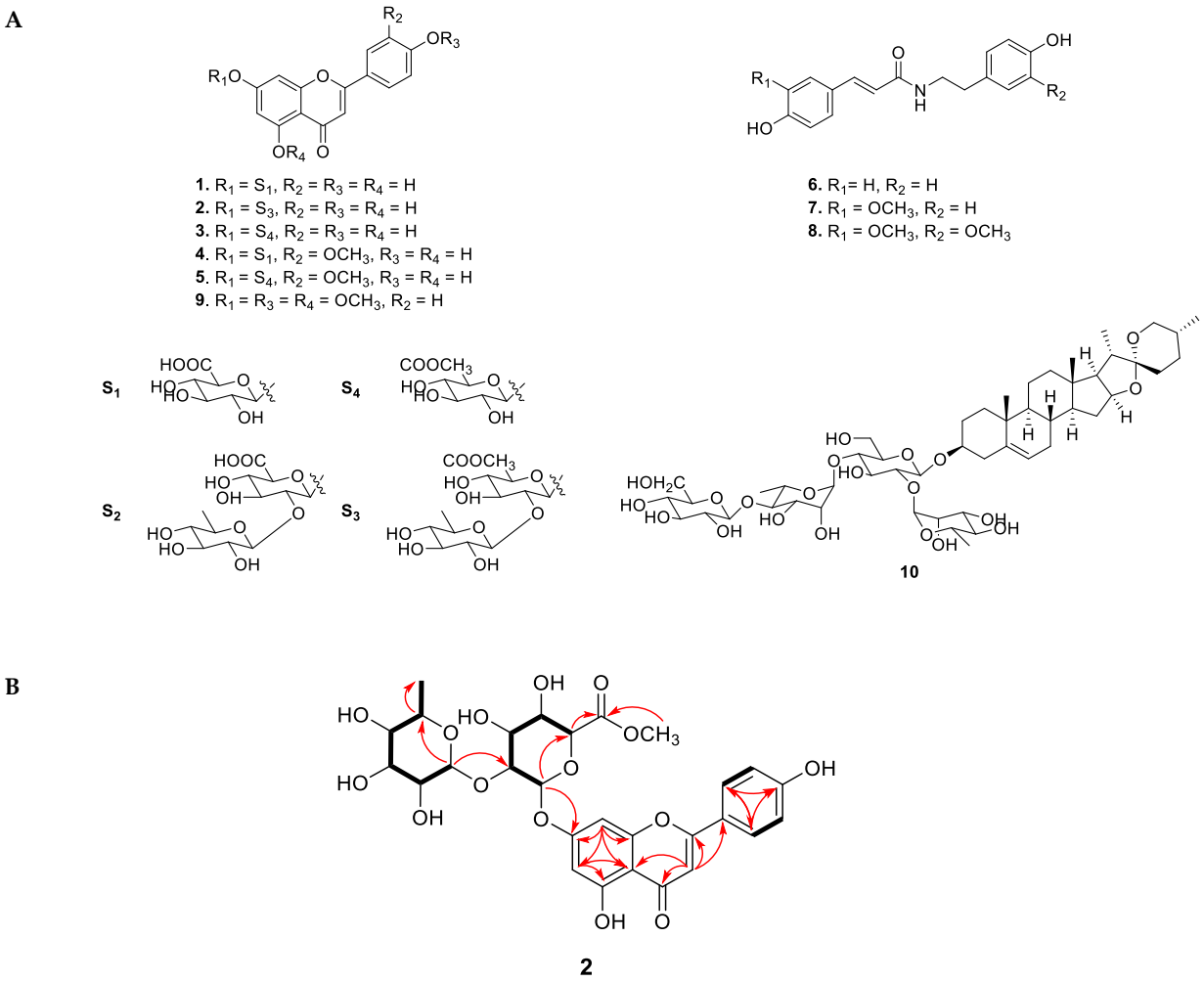

Figure 2. (A) Chemical structures of compounds **1–10** from *A. hookeri*. (B) Key COSY (bold) and HMBC (red arrows) correlations of new compound **2** isolated from *A. hookeri*.

Preprints (www.preprints.org) | NOT PEER-REVIEWED | Posted: 17 October 2023 doi:10.20944/preprints202310.1019.v1

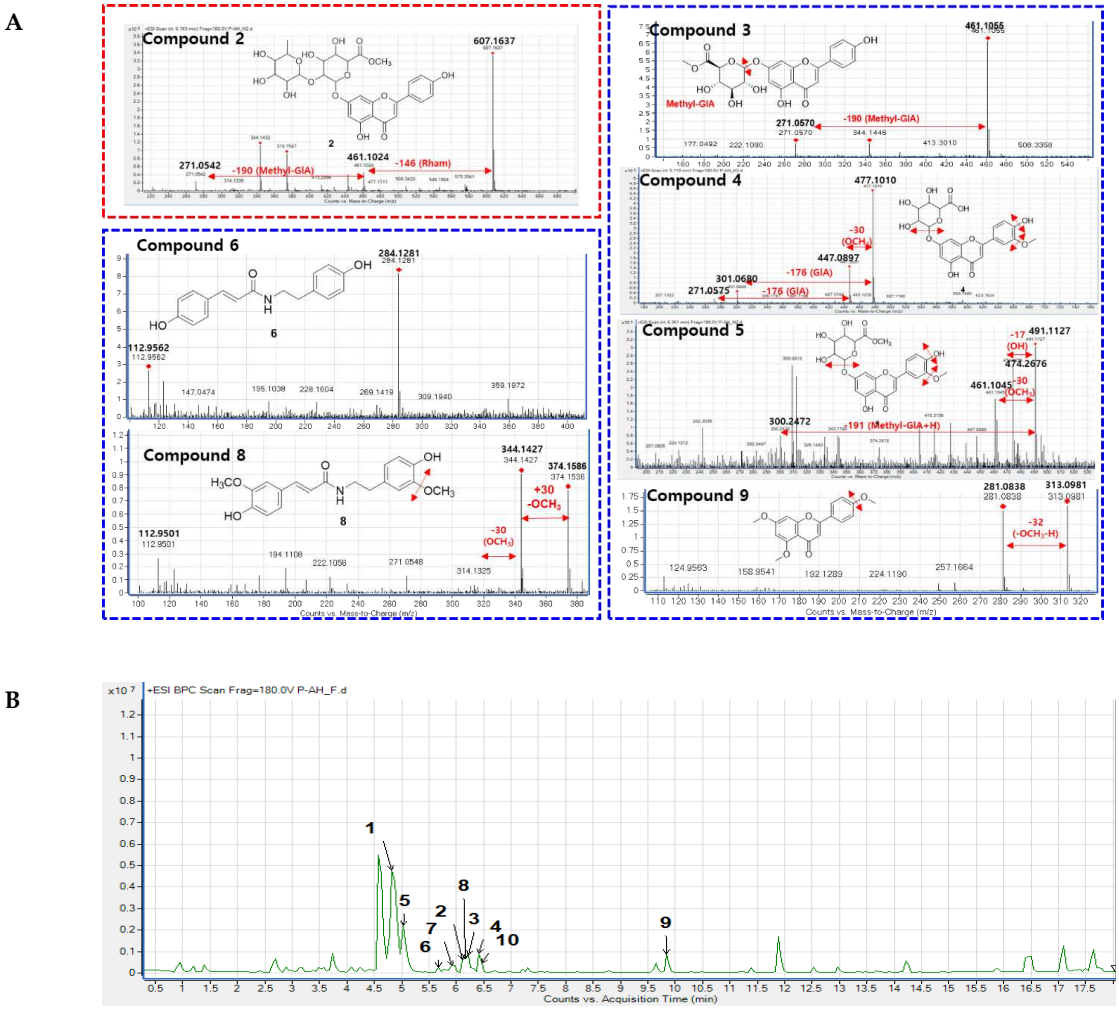

Figure 3. (**A**) Fragmentation analysis of isolated compounds. (**B**) Chemical profiling of isolated compounds in the *A. hookeri* leaves extract. Base peak chromatogram (BPC) of *Allium hookeri* leaves recorded by HRESI-qTOF-MS/MS (positive mode). Compounds **1–10** were marked in the feature-based molecular networking displayed in Figure 1 and their structures were shown in Figure 2.

An analysis of the fragmentation of **7** suggested that it contained a methoxy unit due to the observation of a *m*/*z* 30 Da (-OCH_3) loss. Following isolation, NMR elucidation, and comparison with the literature, **7** was identified as the same as the GNPS assignment of N-*trans*-feruloyltyramine [30]. Compound **6** (*m*/*z* 284 Da) was located in the same cluster as **7** and showed a 30 Da mass difference, indicating the absence of the methoxy group compared to **7**. Compound **6** was isolated, and its NMR confirmed the suggested its structure as paprazine [31]. Compound **8** (*m*/*z* 344 Da) suggested the presence of an additional methoxy compared to **7**. The NMR of **8** was analyzed and compared with previous reports to identify it as *N*-trans-feruloyl-3-*O*-methyldopamine [31].

In the triterpenoids cluster, compound **10** (*m*/*z* 1031 Da) was suggested to be diosgenin-3-*O*-[[β-D-glucopyranosyl(1 → 4)]-α-L-rhamnopyranosyl(1 → 4)]-[α-L-rhamnopyranosyl(1 → 2)]]β-D-glucopyranoside. The mass fragmentation analysis agreed with the presence of two rhamose (Rham) units, as evidenced by the mass loss at *m*/*z* 146 Da. It also contained two glucose (Glc) moieties, as indicated by the mass loss of *m*/*z* 162 Da. After isolation, NMR analysis, and comparison to previous reports, the structure of **10** was confirmed to be annotated [32]. Within this cluster, two nodes with *m*/*z* values of 1033 Da were observed, differing by two hydrogens from compound **10**, yet sharing identical fragments including those at 577, 739, and 885 Da. Mass loss analysis of these nodes indicated the presence of 2 Glc (-162 Da), 1 Rham (– 146 Da), and an Arabinose (Ara, – 148 Da). This information allows for two possible structural configurations, as displayed in Figure S4A

 doi:10.20944/preprints202310.1019.v1

(Supplementary Materials). Similarly, a node at 869.4894 Da within the same cluster displayed fragments indicative of mass losses corresponding to two Rham (146 Da) and a Glc (162 Da). Compared to compound **10**, this node exhibited a mass difference of 162 Da, suggesting the presence of an additional Glc. Consequently, this structure can be assigned to one of nine potential configurations, as illustrated in Figure S4B (Supplementary Materials). Furthermore, within this cluster, two nodes were identified at *m*/*z* 723.4238 and 723.4296 Da (with retention times of 8.15 and 13.36 minutes, respectively), indicating a 308 Da mass difference [= 162 (Glc) + 146 (Rham)] in comparison to compound **10**. Mass fragmentation analysis of these two peaks was conducted and searched in Scifinder, revealing 19 possible structural candidates (Figure S4C and D, Supplementary Materials). These predicted compounds vary in their absolute configurations, which cannot be discerned solely through mass analysis.

3.2. Isolation and Structural Elucidation of New Compound 2

The leaves of *A. hookeri* were extracted by 70% EtOH (3 times) to obtain the total crude extract. The crude extract was further applied to various column chromatography methods to isolate ten compounds, including one new compound (**2**) and nine known compounds (**1**, **3**–**10**), as shown in Figure 1. The chemical structures of known compounds were confirmed by mass analysis and comparison with previous reports, as mentioned above.

Compound **2** was obtained as a pale yellow powder with an established molecular formula of $C_{28}H_{30}O_{15}$, based on its negative HRESIMS at 605.1437 $[M-H]^-$ (calcd for $C_{28}H_{29}O_{15}$ at 605.1585). In the FBMN, compound **2** was observed in a cluster of flavonoid-glycosides, suggesting that the structure of **2** has the same skeleton as identified flavonoid-glycosides. As shown in Figure 3, mass fragmentation of **2** indicated that it contained one Rham (*m*/*z* 146 Da) and one methyl-GlA (*m*/*z* 190 Da) unit. The ^{1}H NMR spectrum of **2** showed five aromatic proton signals at δ_H 7.85 (2H, d, J = 5.1 Hz), 7.20 (overlap), 7.19 (2H, overlap), 7.04 (1H, s), one olefinic proton at δ_H 6.93 ppm, two anomeric signals at δ_H 5.44 (1H, d, J = 7.5 Hz) and 5.11 (1H, d, J = 1.8 Hz), six oxygenated protons [δ_H 4.65, t (7.8); 4.47, t (8.8); 4.52, t (8.8); 4.88, d (8.5); 4.84, br s; 4.58, d (7.7); 4.38, t (9.1); 4.80, m], one methoxy group (δ_H 3.90, s) and one methyl group [δ_H 1.18, d, (6.3)]. The ^{13}C NMR data of **2** displayed 28 carbon signals, including one ketone (δ_C 183.3), an ester carbon (δ_C 170.4), fourteen aromatic signals (δ_C 100.8–165.5), two anomeric carbons (δ_C 100.0, 95.6), eight carbons bearing oxygen (δ_C 70.6–78.7), and one methyl (δ_C 19.4). The HMBC data of **2** confirmed the presence of a flavone moiety by the correlations in the two aromatic rings (Figure 2B). The glucuronic acid attached to C-7 of the flavone moiety was revealed by the cross-peaks from H-1′ (δ_H 6.03, d, J = 7.3 Hz) to C-7 (δ_C 163.7). The methoxy group attached to C-3′ was confirmed by the correlation from the methoxy proton signal (δ_H 3.89, s) to aromatic carbon at δ_C 148.8 ppm. The rhamnose sugar moiety was identified by the presence of a methyl group (δ_H 1.18, d, (6.0)/ δ_C 18.0 ppm) and its correlation with carbon signals of sugar at δ_C 69.4 and 73.0 ppm. The position of rhamnose moiety was represented by the correlation from H-1‴ (δ_H 6.45 ppm) to C-2″ (δ_C 77.8 ppm). The absolute configuration of the sugar unit was determined following acid hydrolysis and compared with the authentic sugar. The retention time of the sugar derivative n **2** was consistent with that of authentic sugar. Therefore, the structure of **2** was identified as shown in Figure 2, and named apigenin-7-*O*-[*α*-L-rhamnopyranosyl(1→2)]*β*-D-glucuronic acid methyl ester.

3.4. Bio-Activity of Isolated Compounds from A. hookeri

In our assay system, senescent human dermal fibroblast (HDF) or lung fibroblast (IMR-90) cells were induced by replicative exhaustion. SA-*β*-gal activity and SASP secretion were used to evaluate senomorphics activity. Positive SA-*β*-gal staining and overexpression of SASP factors such as IL-6, IL-8, and IL-1*α* were confirmed in replicative senescent HDF cells. Drugs that reduced SA-*β*-gal staining or inhibited expression of these SASP factors are thought to be senomorphics candidates.

Ten isolated compounds (**1**–**10**) from *A. hookeri* were evaluated for their capacity in reducing NO production. The cell viability of these compounds was tested at 5 and 20 *μ*M on LPS-induced NO production in RAW 264.7 cells compared to quercetin, a positive control. As a result, all compounds

Preprints (www.preprints.org) | NOT PEER-REVIEWED | Posted: 17 October 2023 doi:10.20944/preprints202310.1019.v1

did not show any cytotoxicity up to 20 μM (Figure 4A), and among them, compound **6** showed the best effect in reducing NO production (Figure 4B). In addition, compounds **6–8** shared similar structures, so their senomorphic effects in bleomycin (BLM)-senescent A549 cells were further evaluated. Two SASP markers, IL-6 and IL-8, were used to test senomorphic activity. As shown in Figure 5A,B, compounds **6–8** reduced the expression of both IL-6 and IL-8 in stress-induced senescent A549 cells that were exposed to 5 μM of BML after 6 days of treatment. The dose-dependent manner of each compound was also tested, and all compounds **6–8** were found to have senomorphic effects by decreasing the expression of IL-6 and IL-8 (Figure 5B). After 6 days of treatment, the SA-β-gal staining was significantly reduced by 10 μM of all three compounds without any detected toxicity (Figure 5C). Furthermore, the SASP inhibitory activities of **6–8** in replicative senescent HDF cells were tested. The compounds were treated at 10 μM on replicative senescent HDF cells, which were confirmed to be senescence by positive SA-β-gal staining (Figure S52, Supplementary Materials) and upregulated SASP makers including IL-1α and IL-8. After 72 h of treatment, compounds **6–8** significantly reduced the expression of IL-1α and IL-8 (Figure 6A,B). Among them, compound **7** showed the best effect in replicative senescent HDF cells in a dose-dependent manner. As a result, compound **7** showed senomorphic activities in replicative senescent HDF cells at 5 and 10 μM by significantly reducing both IL-1α and IL-8 expression levels (Figure 6C,D).

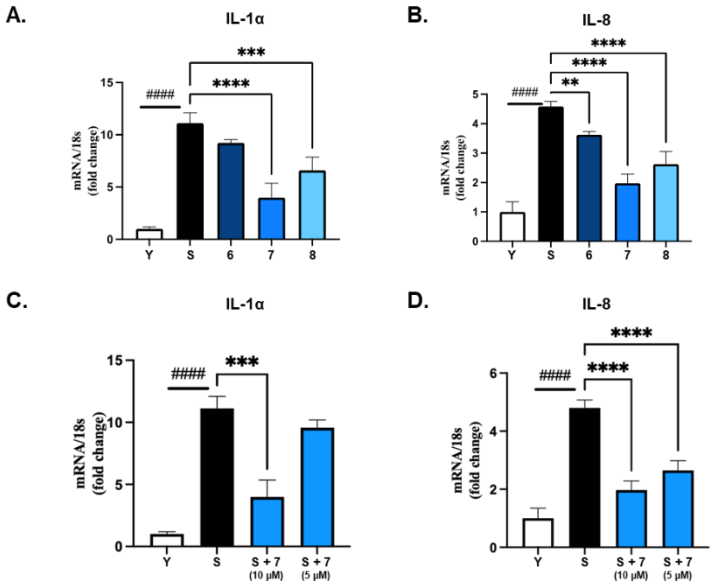

Figure 6. SASP inhibitor in replicative senescent HDF cells of compounds **6–8** from *A. hookeri*. 10μM of compounds **6–8** were treated on replicative senescent HDF which was confirmed by positive SA-β-gal staining (Figure S43) and upregulated SASP factors such as IL-1α and IL-8. (**A**) and (**B**) compounds **6–8** significantly reduced expression of IL-1α or IL-8 after 72 h treatment and compound **7** shows the best effect among them. (**C**) and (**D**) compound **7** was tested to have senomorphic effect in replicative senescent HDF cells in a dose-dependent manner. Data are presented as the mean ± SDs (n = 3), one-way ANOVA with Dunnett's Multiple Comparison, ** $p < 0.01$, *** $p < 0.001$ and **** $p < 0.0001$ compared to the control samples; t-test, $^{\#\#\#\#}$ $p < 0.0001$.

Preprints (www.preprints.org) | NOT PEER-REVIEWED | Posted: 17 October 2023 doi:10.20944/preprints202310.1019.v1

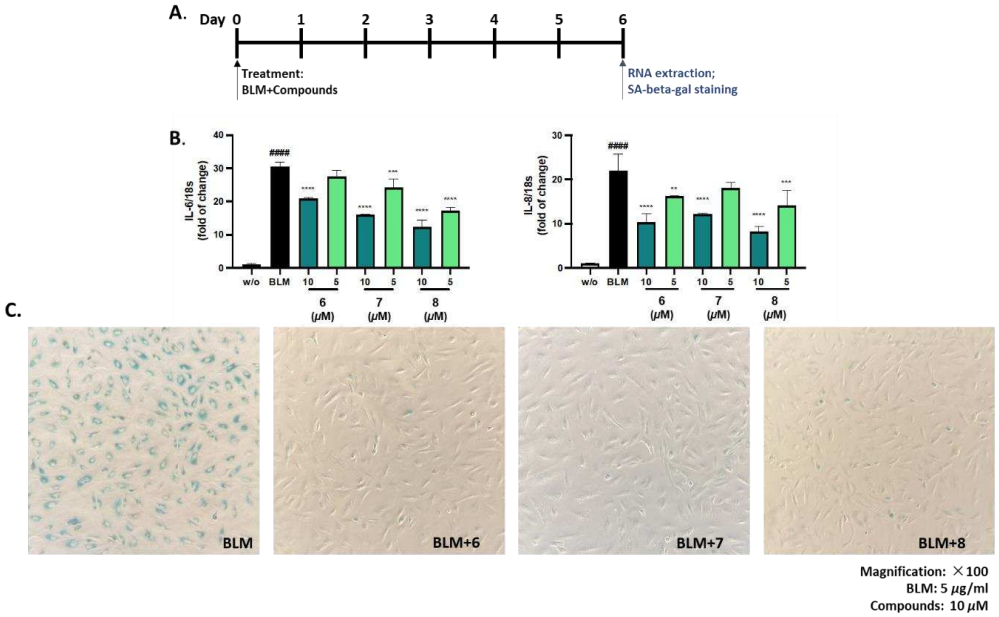

Figure 5. Senomorphic effects in BLM-senescent A549 cells of compounds **6**–**8** from *A. hookeri*. (**A**) A549 cells were exposed to 5 μg/ml of Bleomycin (BML) and co-treated with indicated compounds for 6 days. Then, cells were analyzed by RNA extraction or SA-β-gal staining. (**B**) Compounds **6–8** were tested in a dose-dependent manner and all three compounds showed senomorphic effects by decreasing the expression of IL-6 and IL-8 in stress-induced senescent cells. (**C**) After 6 days of treatment, SA-β-gal staining was significantly reduced by 10 μM of all those compounds and no severe toxicity was detected. Data are presented as the mean ± SDs (n = 3), one-way ANOVA with Dunnett's Multiple Comparison, $^{**}p < 0.01$, $^{***}p < 0.001$ and $^{****}p < 0.0001$ compared to the control samples; t-test, $^{\#\#\#\#}p < 0.0001$.

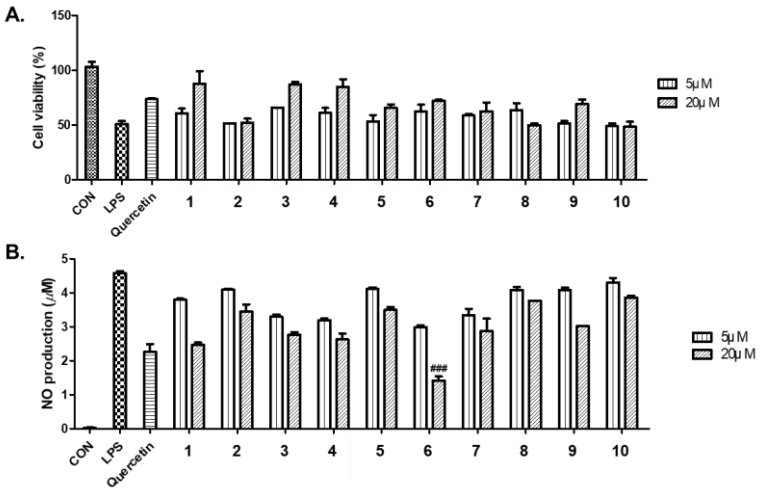

Figure 4. (**A**) Cell viability of compounds **1–10** from *A. hookeri* was measured using the EZ-Cytox cell viability assay. (**B**) Inhibitory effects of compounds **1–10** on LPS-induced NO production in RAW 264.7 cells compared to quercetin used as a positive control. Cell viability data represent relative cell viability compared with that of the untreated group (100%). NO assay data represent NO production levels calculated by applying absorbance values at 540 nm to a nitrite standard curve (white bar, untreated control group; black bar, LPS-treated control group); $p < 0.05$ relative to the LPS-treated control group.

4. Discussion

In this study, we report the isolation and characterization of one new compound (**2**) from *A. hookeri*, along with nine known compounds (**1**, **3–10**). We evaluated the senomorphic effects of all the isolated phytochemicals, characterized by a reduction in SASP markers, including IL-6, IL-8, and IL-1α, as well as SA-β-gal staining. Our results indicate that *N-trans*-feruloyltyramine exhibits the most promising SASP-inhibitory activity among the isolated compounds. Notably, this is the first report of the senomorphic activity of *N-trans*-feruloyltyramine, which has previously been demonstrated to possess a wide range of biological effects, such as protection against scopolamine-induced cholinergic dysfunction on the cortex and hippocampus [33] and β-amyloid peptide-induced neurotoxicity [34], inhibition of melanin biosynthesis [35], antioxidant, cytotoxic activities, and protection against H2O2-induced oxidative damage [36].

Of particular interest, the active compounds (**6–8**) shared a similar skeleton with avenanthramide C (Avn C), with the only difference being the phenyl ethyl moieties of **6–8** and unit of benzoic acid of avenanthramide C. Avenanthramide C has recently been extensively studied for its protective effects against pediatric pneumonia [37], allergic inflammation [38], its senomorphic effect [39], and its ability to restore impaired plasticity and cognition in mice model of Alzheimer's disease [40]. *In vitro* results from those studies suggested that Avn C reduces cytokines including IL-4 [38], IL-6 [38,39], IL-8 [39], TNF-α [38,39], and SASP [39]. These findings are consistent with the present study's data, which demonstrate the potential of phenolamides from *A. hookeri* to inhibit SASP in senescent cells and contribute to their senomorphic activities. Hence, its natural amide skeleton could be a promising analog for developing drugs to treat age-related diseases.

5. Conclusions

In summary, our study utilized HRESI-qTOF-MS/MS-based molecular networking to profile the phytochemicals in *A. hookeri* leaves. The molecular networking analysis revealed the presence of flavonoid-glycosides, flavonoids-aglycone, triterpenoids, and phenolamides. Subsequently, we isolated and identified ten compounds from *A. hookeri* leaves, including one new flavonoid and nine known compounds, through NMR analysis. These compounds were then evaluated for their effects on senescent cell-associated secretory phenotype (SASP), a key contributor to neuroprotective activities. Notably, compound *N-trans*-feruloyltyramine (**7**) exhibited the highest potency in inhibiting SASP markers, underscoring its significance in the senomorphic activities of *A. hookeri*. These findings highlight the potential of phenolamides from *A. hookeri* as a valuable source of bioactive compounds for mitigating senescence-associated diseases.

Supplementary Materials: The following are available online at www.mdpi.com/xxx/s1, Figure S1: title, Table S1: title, Video S1: title. **Figure S1.** HR-ESI -qTOF-MS/MS chromatography of *A. hookeri* leaves extract (positive mode), **Figure S2**: Feature-based molecular networking of fractions and crude extract from leaves of *Allium hookeri* using HRESI-qTOF-MS/MS. Mass data was recorded in positive mode, **Figure S3.** Chemical structures of putative identification of components from leaves of *Allium hookeri* using HRESI-qTOF-MS/MS-based molecular networking, **Figure S4**. Mass/mass fragmentation of triterpenoid cluster in FBMN, **Figure S5**. HRESIMS data of compound **2, Figure S6.** IR(KBr) spectrum of compound **2**, **Figure S7**. ^{1}H NMR spectrum of compound **2** (600 MHz, pyridine-d_5), **Figure S8**. ^{13}C NMR spectrum of compound **2** (150 MHz, pyridine-d_5), **Figure S9**. HSQC spectrum of compound **2, Figure S10.** HMBC spectrum of compound **2**, **Figure S11.** COSY spectrum of compound **2, Figure S12.** HRESIMS/MS of compound **1, Figure S13.** IR(KBr) spectrum of compound **1**, **Figure S14**. ^{1}H NMR spectrum of compound **1** (400 MHz, DMSO-d_6), **Figure S15**. HRESIMS/MS of compound **3, Figure S16.** IR(KBr) spectrum of compound **3**, **Figure S17**. ^{1}H NMR spectrum of compound **3** (600 MHz, DMSO-d_6), **Figure S18.** ^{13}C NMR spectrum of compound **3** (150 MHz, DMSO-d_6), **Figure S19**. HRESIMS data of compound **4, Figure S20.** UV spectrum of compound **4**, **Figure S21**. IR(KBr) spectrum of compound **4, Figure S22.** ^{1}H NMR spectrum of compound **4** (500MHz, DMSO-d_6), **Figure S23**. ^{13}C NMR spectrum of compound **4** (125 MHz, DMSO-d_6), **Figure S24.** HRESIMS data of compound **5**, **Figure S25.** UV spectrum of compound **5**, **Figure S26.** IR(KBr) spectrum of compound **5**, **Figure S27**. ^{1}H NMR spectrum of compound **5** (600 MHz, DMSO-d_6), **Figure S28**. ^{13}C NMR spectrum of compound **5** (150 MHz, DMSO-d_6), **Figure S29**. HRESIMS data of compound **6, Figure S30.** IR(KBr) spectrum of compound **6**, **Figure S31**. ^{1}H NMR spectrum of compound **6** (500 MHz, DMSO-d_6), **Figure S32.** ^{13}C NMR spectrum of compound **6** (125 MHz, DMSO-d_6), **Figure S33.** HRESIMS data of compound **7**, **Figure S34**. IR(KBr) spectrum of compound **7, Figure S35.** ^{1}H NMR spectrum of compound **7** (400 MHz, DMSO-d_6),

Figure S36. ^{13}C NMR spectrum of compound **7** (100 MHz, DMSO-d_6), **Figure S37.** HRESIMS data of compound **8**, **Figure S38**. UV spectrum of compound **8**, **Figure S39**. IR(KBr) spectrum of compound **8**, **Figure S40**. ^{1}H NMR spectrum of compound **8** (600 MHz, DMSO-d_6), **Figure S41**. ^{13}C NMR spectrum of compound **8** (150 MHz, DMSO-d_6), **Figure S42**. HRESIMS/MS data of compound **9, Figure S43.** UV spectrum of compound **9, Figure S44.** IR(KBr) spectrum of compound **9, Figure S45.** ^{1}H NMR spectrum of compound **9** (600 MHz, DMSO-d_6), **Figure S46.** ^{13}C NMR spectrum of compound **9** (150 MHz, DMSO-d_6), **Figure S47.** HRESIMS/MS data of compound **10, Figure S48.** IR(KBr) spectrum of compound **10**, **Figure S49.** ^{1}H NMR spectrum of compound **10** (500 MHz, pyridine-d_5), **Figure S50.** ^{13}C NMR spectrum of compound **10** (125 MHz, pyridine-d_5), **Figure S51**. Inhibitory effects of fractions and single compounds from *A. hookeri* on BLM-induced senescence system in RAW 264.7 cells using nitric oxide (NO) assay kit, **Figure S52.** SA-β-gal-positive senescent cells on replicative senescent HDF cell, **Table S1**. Putative identification of components from leaves of *Allium hookeri* using HRESI-qTOF-MS/MS-based molecular networking. **.**

Author Contributions: Conceptualization and Methodology, T.P.D., J.P.A. and M.Z.; Investigation, T.P.D., M.Z., and E.J.P, Re-sources, J.E.P. and V.H.M.; Data curation, T.P.D., M.Z., and B.R.; Writing—original draft preparation, T.P.D., M.Z.; Writing—review and editing, T.P.D. and W.K.O.; Visualization, T.P.D. and M.Z., Super-vision, Project administration, and Funding acquisition, W.K.O. All authors have read and agreed to the published version of the manuscript

Funding: This research was supported by grants from the Cooperative Research Program for Agriculture Science and Technology Development (Project No. PJ017134) through Rural Development Administration and from the Basic Science Research Program (NRF-2022R1A2C2005061) through the National Research Foundation of Korea (NRF) funded by the Korean government (MSIT).

Conflicts of Interest: The authors declare no conflict of interest

References

1. Fenwick, G.R.; Hanley, A.B.; Whitaker, J.R. The Genus *Allium* . Part 2. *CRC Crit. Rev. Food Sci. Nutr*. **1985**, *22*, 273–377.
2. Sabiu, S.; Madende, M.; Ajao, A.A.; Aladodo, R.A.; Nurain, I.O.; Ahmad, J.B. Chapter 9: The Genus *Allium* (Amaryllidaceae: Alloideae): Features, Phytoconstituents, and Mechanisms of Antidiabetic Potential of *Allium cepa* and *Allium sativum*. *Bioactive Food as Dietary Interventions for Diabetes,* Academic Press, Cambridge: The USA, 2019; pp. 137–154.
3. Bae, G.C.; Bae, D.Y. The Anti-Inflammatory Effects of Ethanol Extract of *Allium hookeri* Cultivated in South Korea. *Kor. J. Herbology* **2012**, *27*, 55–61.
4. Bok, S.; Seo, J.; Bae, C.; Kang, B.; Cho, S.; Park, D. *Allium hookeri* Root Extract Regulates Asthmatic Changes through Immunological Modulation of Th1/Th2-related Factors in an Ovalbumin-induced Asthma Mouse Model. *Mol. Med. Rep*. **2019**, *20*, 3215–3223.
5. Jun, H.I.; Jang, H.; Ahn, D.; Kim, D.K.; Yang, J.H.; Yun, B.S.; Kim, Y.S. Isolation and Characterization of Phenolic Compound from *Allium hookeri* Root for Potential Use as Antioxidant in Foods. *Food Sci. Biotechnol*. **2015**, *24*, 2031–2034.
6. Kim, J.E.; Seo, J.H.; Bae, M.S.; Bae, C.S.; Yoo, J.C.; Bang, M.A.; Cho, S.S.; Park, D.H. Antimicrobial Constituents from *Allium hookeri* Root. *Nat. Prod. Commun*. **2016**, *11*, 237–238.
7. Roh, S.S.; Kwon, O.J.; Yang, J.H.; Kim, Y.S.; Lee, S.H.; Jin, J.S.; Jeon, Y.D.; Yokozawa, T.; Kim, H.J. *Allium hookeri* Root Protects Oxidative Stress-Induced Inflammatory Responses and β-Cell Damage in Pancreas of Streptozotocin-Induced Diabetic Rats. *BMC Complement Altern. Med*. **2016**, *16*, 1–10.
8. Park, S.H.; Bae, U.J.; Choi, E.K.; Jung, S.J.; Lee, S.H.; Yang, J.H.; Kim, Y.S.; Jeong, D.Y.; Kim, H.J.; Park, B.H.; et al. A Randomized, Double-Blind, Placebo-Controlled Crossover Clinical Trial to Evaluate the Anti-Diabetic Effects of *Allium hookeri* Extract in the Subjects with Prediabetes. *BMC Complement Med. Ther*. **2020**, *20*, 1–8.
9. Lee, Y.; Hyen Lee, S.; Sun Jeong, M.; Kim, J.B.; Hee Jang, H.; Choe, J.; Kim, D.W.; Lillehoj, H.S. In Vitro Analysis of the Immunomodulating Effects of *Allium hookeri* on Lymphocytes, Macrophages, and Tumour Cells. *J. Poult. Sci*. **2017**, *54*, 142–148.
10. Jang, J.Y.; Lee, M.J.; You, B.R.; Jin, J.S.; Lee, S.H.; Yun, Y.R.; Kim, H.J. *Allium hookeri* Root Extract Exerts Anti-Inflammatory Effects by Nuclear Factor-KB down-Regulation in Lipopolysaccharide-Induced RAW264.7 Cells. *BMC Complement Altern. Med*. **2017**, *17*, 1–9.
11. Kim, H.; Rho, S.H.; Lim, J.; Park, H.J.; Jeong, H. Protective Effect of Linoleic Acid against Inflammatory Reactions by Mast Cell via Caspase-1 Cascade Pathways. *J. Food Biochem*. **2019**, *43*, 1–9.
12. Park, H.; Jeong, J.; Hyun, H.; Kim, J.; Kim, H.; Oh, H.; Choi, J.; Hwang, H.; Oh, D.; Kim, J.; et al. Effects of a Hot-Water Extract of *Allium hookeri* Roots on Bone Formation in Human Osteoblast-Like MG-63 Cells In Vitro and in Rats In Vivo. *Planta Med*. **2016**, *82*, 1410–1415.

13. Park, S.; No, K.; Lee, J. Anti-Obesity Effect of *Allium hookeri* Leaf Extract in High-Fat Diet-Fed Mice. *J. Med. Food*. **2018**, *21*, 254–260.
14. Yang, M.H.; Kim, N.H.; Heo, J.D.; Rho, J.R.; Ock, K.J.; Shin, E.C.; Jeong, E.J. Comparative Evaluation of Sulfur Compounds Contents and Antiobesity Properties of *Allium hookeri* Prepared by Different Drying Methods. *Evid. Based Complement Alternat. Med.* **2017**, *2017*, 1–10.
15. Hwang, J.S.; Lee, B.H.; An, X.; Jeong, H.R.; Kim, Y.E.; Lee, I.; Lee, H.; Kim, D.O. Total Phenolics, Total Flavonoids, and Antioxidant Capacity in the Leaves, Bulbs, and Roots of *Allium hookeri*. *Korean J. Food Sci. Technol*. **2015**, *47*, 261–266.
16. Park, S.Y.; Je, J.Y.; Ahn, C.B. Phenolic Composition and Hepatoprotective Activities of *Allium hookeri* Against Hydrogen-Peroxide-Induced Oxidative Stress in Cultured Hepatocytes. *J. Food Biochem*. **2016**, *40*, 284–293.
17. Li, R.; Wang, Y.F.; Sun, Q.; Hu, H. Bin Chemical Composition and Antimicrobial Activity of the Essential Oil from *Allium hookeri* Consumed in Xishuangbanna, Southwest China. *Nat. Prod. Commun*. **2014**, *9*, 863–864.
18. Thiyagarajan, J.A.; Mikton, C.; Harwood, R.H.; Gichu, M.; Gaigbe-Togbe, V.; Jhamba, T.; Pokorna, D.; Stoevska, V.; Hada, R.; Steffan, G.S.; et al. The UN Decade of Healthy Ageing: Strengthening Measurement for Monitoring Health and Wellbeing of Older People. *Age Ageing*. **2022**, *51*, 1–5.
19. Beard, J.R.; Officer, A.; de Carvalho, I.A.; Sadana, R.; Pot, A.M.; Michel, J.-P.; Lloyd-Sherlock, P.; Epping-Jordan, J.E.; Peeters, G.M.E.E. (Geeske); Mahanani, W.R.; et al. The World Report on Ageing and Health: A Policy Framework for Healthy Ageing. *The Lancet* **2016**, *387*, 2145–2154.
20. Boccardi, V.; Mecocci, P. Senotherapeutics: Targeting Senescent Cells for the Main Age-Related Diseases. *Mech. Ageing. Dev*. **2021**, *197*, 111526.
21. Sun, Y.; Coppé, J.P.; Lam, E.W.F. Cellular Senescence: The Sought or the Unwanted? *Trends Mol. Med*. **2018**, *24*, 871–885.
22. van Deursen, J.M. The Role of Senescent Cells in Ageing. *Nature*. **2014**, *509*, 439–446.
23. Li, W.; Qin, L.; Feng, R.; Hu, G.; Sun, H.; He, Y.; Zhang, R. Emerging Senolytic Agents Derived from Natural Products. *Mech. Ageing Dev*. **2019**, *181*, 1–6.
24. Luís, C.; Maduro, A.T.; Pereira, P.; Mendes, J.J.; Soares, R.; Ramalho, R. Nutritional Senolytics and Senomorphics: Implications to Immune Cells Metabolism and Aging – from Theory to Practice. *Front Nutr*. **2022**, *9*, 1–15.
25. Lee, Y.; Kim, H.M.; Kim, J.H.; Lee, J.-H.; Zhang, K.X.; Gao, E.M.; Jeon, J.-S.; Syed, A.S.; Son, R.H.; Kim, J.-Y.; et al. Chemical Constituents of the *Ajuga Multiflora* Bunge and Their Protective Effects on Dexamethasone-Induced Muscle Atrophy in C2C12 Myotubes. *Nat. Prod. Res*. **2023**, *37*, 1978–1985.
26. Lehbili, M.; Alabdul Magid, A.; Kabouche, A.; Voutquenne-Nazabadioko, L.; Abedini, A.; Morjani, H.; Gangloff, S.C.; Kabouche, Z. Antibacterial, Antioxidant and Cytotoxic Activities of Triterpenes and Flavonoids from the Aerial Parts of *Salvia Barrelieri* Etl. *Nat. Prod. Res*. **2018**, *32*, 2683–2691.
27. Myagchilov, A. V.; Gorovoi, P.G.; Sokolova, L.I. Flavonoids from *Serratula komarovii* Iljin (the Asteraceae Family). *Russ. J. Bioorg. Chem*. **2021**, *47*, 1418–1423.
28. Yanting, L.R.J.B.X.Z. Chrysoeriol-7-O-Beta-D Glucuronic Acid Methyl Ester and Extraction Method and Application Thereof. **2017**, 1–9. https://worldwide.espacenet.com/patent/search/family/060495965/publication/CN107446009A?q=pn%3DCN107446009A
29. Sutthanut, K.; Sripanidkulchai, B.; Yenjai, C.; Jay, M. Simultaneous Identification and Quantitation of 11 Flavonoid Constituents in *Kaempferia parviflora* by Gas Chromatography. *J. Chromatogr A*. **2007**, *1143*, 227–233.
30. van Zadelhoff, A.; Vincken, J.P.; de Bruijn, W.J.C. Facile Amidation of Non-Protected Hydroxycinnamic Acids for the Synthesis of Natural Phenol Amides. **2022**, *27*.
31. Zheng, Y.; Su, B.; Wang, Y.; Wang, H.; Liao, H.; Liang, D. New Tyramine- and Aporphine-Type Alkamides with NO Release Inhibitory Activities from *Piper puberulum*. *J. Nat. Prod*. **2021**, *84*, 1316–1325.
32. Chen, S.; Snyder, J.K. Diosgenin-Bearing, Molluscicidal Saponins from Allium Vineale: An NMR Approach for the Structural Assignment of Oligosaccharide Units. *J. Org. Chem*. **1989**, *54*, 3679–3689.
33. Thangnipon, W.; Ngampramuan, S.; Suthprasertporn, N.; Jantrachotechatchawan, C.; Tuchinda, P.; Nobsathian, S. Protective Roles of N-*Trans*-Feruloyltyramine Against Scopolamine-Induced Cholinergic Dysfunction on Cortex and Hippocampus of Rat Brains. *Siriraj Med J*. **2021**, *73*, 413–422.
34. Thangnipon, W.; Suwanna, N.; Kitiyanant, N.; Soi-ampornkul, R.; Tuchinda, P.; Munyoo, B.; Nobsathian, S. Protective Role of N-*Trans*-Feruloyltyramine against β-Amyloid Peptide-Induced Neurotoxicity in Rat Cultured Cortical Neurons. *Neurosci. Lett*. **2012**, *513*, 229–232.
35. Efdi, M.; Ohguchi, K.; Akao, Y.; Nozawa, Y.; Koketsu, M.; Ishihara, H. N-Trans-Feruloyltyramine as a Melanin Biosynthesis Inhibitor. *Biol. Pharm. Bull*. **2007**, *30*, 1972–1974.

36. Gao, X.; Wang, C.; Chen, Z.; Chen, Y.; Santhanam, R.K.; Xue, Z.; Ma, Q.; Guo, Q.; Liu, W.; Zhang, M.; et al. Effects of N-*Trans*-Feruloyltyramine Isolated from Laba Garlic on Antioxidant, Cytotoxic Activities and H2O2-Induced Oxidative Damage in HepG2 and L02 cells. **2019**, *130*, 130–141.
37. Pu, Z.; Shen, C.; Zhang, W.; Xie, H.; Wang, W. Avenanthramide C from Oats Protects Pyroptosis through Dependent ROS-Induced Mitochondrial Damage by PI3K Ubiquitination and Phosphorylation in Pediatric Pneumonia. *J. Agric. Food Chem*. **2022**, *70*, 2339–2353.
38. Dhakal, H.; Yang, E.-J.; Lee, S.; Kim, M.-J.; Baek, M.-C.; Lee, B.; Park, P.-H.; Kwon, T.K.; Khang, D.; Song, K.-S.; et al. Avenanthramide C from Germinated Oats Exhibits Anti-Allergic Inflammatory Effects in Mast Cells. *Sci. Rep*. **2019**, *9*, 6884.
39. Lim, J.S.; Lee, D.Y.; Kim, H.S.; Park, S.C.; Park, J.T.; Kim, H.S.; Oh, W.K.; Cho, K.A. Identification of a Novel Senomorphic Agent, Avenanthramide C, via the Suppression of the Senescence-Associated Secretory Phenotype. *Mech. Ageing Dev*. **2020**, *192*, 111355.
40. Ramasamy, V.S.; Samidurai, M.; Park, H.J.; Wang, M.; Park, R.Y.; Yu, S.Y.; Kang, H.K.; Hong, S.; Choi, W.-S.; Lee, Y.Y.; et al. Avenanthramide-C Restores Impaired Plasticity and Cognition in Alzheimer's Disease Model Mice. *Mol. Neurobiol*. **2020**, *57*, 315–330.